Resonant photoemission in *f*-electron systems: Pu and Gd

J. G. Tobin* and B. W. Chung
Lawrence Livermore National Laboratory, Livermore, California, USA

R. K. Schulze, J. Terry, and J. D. Farr
Los Alamos National Laboratory, Los Alamos, New Mexico, USA

D. K. Shuh, K. Heinzelman, and E. Rotenberg
Lawrence Berkeley National Laboratory, Berkeley, California, USA

G. D. Waddill
University of Missouri-Rolla, Rolla, Missouri, USA

G. van der Laan
Daresbury Laboratory, Warrington, WA4 4AD, United Kingdom
(Received 13 March 2003; revised manuscript received 30 June 2003; published 14 October 2003)

Resonant photoemission in the Pu $5f$ and Pu $6p$ states is compared to that in the Gd $4f$ and Gd $5p$ states. Spectral simulations, based upon an atomic model with angular momentum coupling, are compared to the Gd and Pu results. Additional spectroscopic measurements of Pu, including core level photoemission and x-ray absorption, are also presented.

DOI: 10.1103/PhysRevB.68.155109 PACS number(s): 71.20.Gj, 71.27.+a, 79.60.−i

I. INTRODUCTION

While chemically toxic and highly radioactive, Pu may be the most scientifically interesting element in the Periodic Table. It's properties include the following,[1] six different phases, close to each other in energy and sensitive to variations of temperature, pressure and chemistry; the face-centered-cubic phase (delta) is the *least* dense; Pu expands when it solidifies from the melt; and it is clearly the nexus of the actinide binary phase diagram. In a sense, it is the boundary between the light (delocalized $5f$ electrons) and heavy (localized or correlated $5f$ electrons) actinide elements, but this is an oversimplification. The localized atomic $5f$ states are naturally correlated, but important regimes of correlated electron states are conceivable as extended states on the delocalized side of the possible Mott transition. The proximity to this crossover may be the driving force behind these all exotic properties. Pu remains of immense technological importance and the advancement to a firm, scientific understanding of Pu and its compounds, mixtures, alloys and solutions is a crucial issue.[1,2]

As a result, computationally modeling Pu is a challenge. There have been substantial efforts made over the years.[3–5] Some of the more recent work includes pursuit of the structural parameters of alpha Pu from first principal calculations,[6] the electronic and phonon properties of the six phases,[7] the alloy electronic structure,[8] and the effects of localization in the $5f$ states.[9] Of particular interest is the dynamical mean field theory approach[10,11] and the models that predict the possibility of an internal magnetic ordering in the electronic structure.[12,13]

Furthermore, the development of computationally based predictive capabilities hinges upon experimental benchmarking of the variously proposed models. Perhaps the most direct method for testing models of electronic structure is photoelectron spectroscopy. In the recent past, there have been a number of photoelectron spectroscopy studies of Pu, using laboratory sources such as He I (21.22 eV) and He II (40.8 eV). For example, Gouder *et al.* have performed an investigation of $5f$ localization in the PuSe and PuSb.[14,15] Gouder *et al.*[16–18] and Havela *et al.*[19] have also used Pu thin film growth as a means to test for localization in the Pu $5f$ levels. At Los Alamos, a tunable laser plasma source[9,20–22] has been developed by Arko and Joyce, in order to supplement the studies performed with gas discharge lamps.[9] Joyce *et al.*[22] used the laser plasma source to perform a preliminary study of the $5d$-$5f$ resonant photoemission in Pu, but their work was limited by the poor signal to noise ratio of the plasma generated spectra. Earlier x-ray photoelectron spectroscopy included studies of alpha-Pu and delta-Pu by Cox *et al.*[23,24] plutonium metal by Baptist *et al.*,[25] and plutonium oxidation by Couteix *et al.*,[26] Veal *et al.*,[27] and Larson.[28]

This synchrotron-radiation-based study is another important step in such an experimental benchmarking. A summary of our resonant photoemission (RESPES) results for Pu is shown in Fig. 1. By comparing the Pu $5f$ and Pu $6p$ results to a RESPES investigation of the $4f$ system Gd, greater insight will be gained concerning the behavior of $5f$ electrons and Pu. Finally, the results of an atomic model calculation, for both Gd and Pu, will be presented.

II. EXPERIMENTAL AND COMPUTATIONAL DETAILS

The experiments were carried out at the SpectroMicroscopy Facility (Beamline 7.0) (Ref. 29) at the Advanced Light Source in Berkeley, CA, USA. In the photoelectron (x-ray absorption) measurements, the photoelectron (sample current) intensity was normalized to the photon flux by a Au

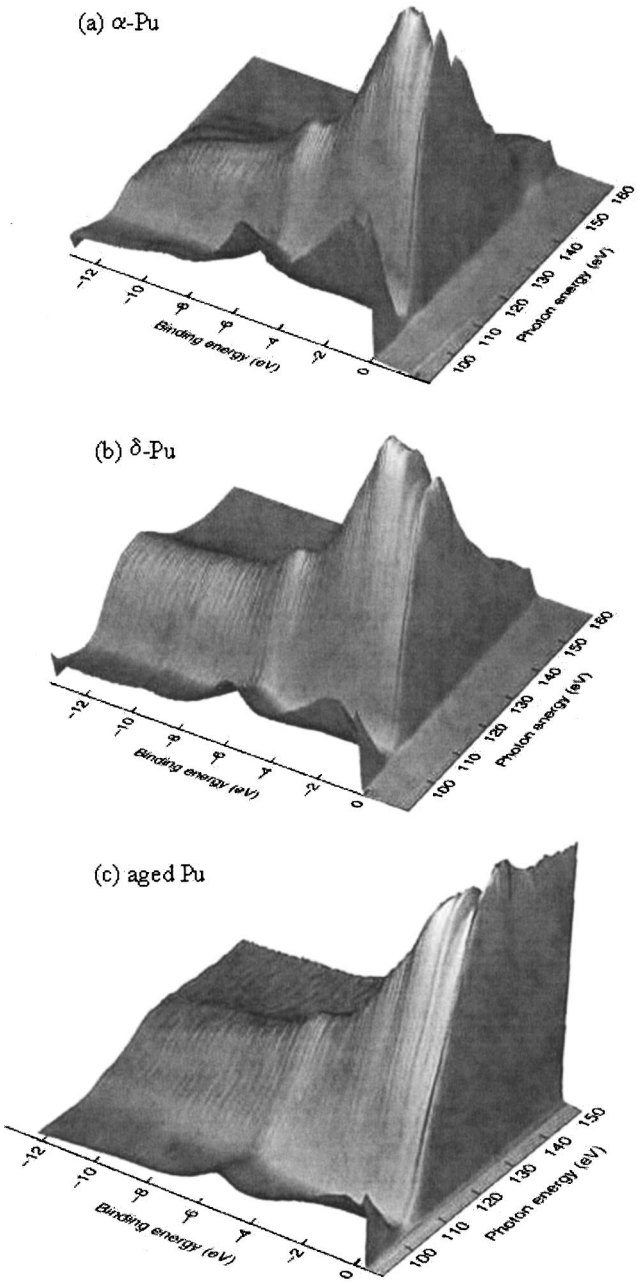

FIG. 1. Resonant photoemission (RESPES) data sets are shown here, for a polycrystalline α (top), single crystallite δ (middle), and aged polycrystalline δ (bottom.) The plots show the intensity variations (z axis) vs the binding energy of the states (the negative numbers in eV; zero is the Fermi energy) and photon energy (between 90 and 160 eV). The alpha sample has been zone refined and is polycrystalline. The delta sample has been prepared by doping the alpha sample material with Ga, and is large crystallite. The aged sample is delta and polycrystalline. These results suggest that RESPES is directly sensitive to changes in valence electronic structure associated with structural and chemical variations. The bandpass was 100 meV or less throughout.

mesh drain current measured upstream.

Epitaxial Gd (0001) metal films approximately 100 Å thick were prepared by *e*-beam evaporation onto a Y(0001) substrate at room temperature. Details of Gd sample preparation, data collection, and a preliminary report of our results can be found in Ref. 30 and references therein. The angle resolved photoemission spectra were collected in the chiral geometry using a Perkin Elmer hemispherical energy analyzer with $+/-2$ degree acceptance angle and an energy resolution of 250 meV. MLDAD spectra are recorded by reversing the magnetization perpendicular to the plane containing the incident linear light polarization and the detected photoemission, which have a mutual angle of 30°.

The Pu spectroscopy experiments were performed upon three bulk Pu samples, each having a mass of approximately 30 mg. Two of the samples were new and highly purified; the third was an aged, less purified sample. The new Pu samples were taken from a specially purified batch of Pu metal. (Ref. 31, and references therein). The plutonium was zone refined and vacuum distilled while being magnetically levitated. The product of the purification process was α-Pu containing a total of 170-ppm wt impurities. A portion of the refined metal was alloyed with gallium to form the δ phase (fcc symmetry). The sample surfaces were prepared by repeated room-temperature, sputter-annealing cycles to minimize the amount of oxygen and other impurities dissolved in the sample or at grain boundaries, in a specially designed chamber attached to the sample introduction and analysis systems on Beamline 7.0. The pressure in the main analysis chamber is typically in the low 10^{-10}-Torr range. In the transfer process, the Pu clean metal samples experienced pressures on the scale of 10^{-8} torr only briefly. Thus, any surface contamination that could adversely affect the soft x-ray measurements was minimized. Unless otherwise specified, the valence band spectra were collected with an energy bandpass of 100 meV or better and the wide scans and core level spectra had a bandpass on the order of 350 meV.

For the Gd and Pu, the transition probability for resonant photoemission was calculated using the *t*-matrix approach in first order in the dipole operator and infinite order in the Coulomb decay. These calculations were done in intermediate coupling using Cowan's relativistic Hartree-Fock code. The interference between the direct photoemission channel and the x-ray absorption Coulomb decay channel was explicitly taken into account by a diagonalization of the Hamiltonian for the connected final state. (Only for the Gd $5p$ emission is the interference excluded in order to reduce the overall size of the calculation.)

The Coulomb decay gives rise to a typical decay halfwidth

$$\Gamma_i = \pi^\star V^2, \tag{1}$$

where V is the Coulomb (or super-Coster-Kronig) matrix element, which is proportional to the radial integrals. The interference with the direct photoemission continuum leads to a typical line asymmetry given by a Fano asymmetry parameter,

$$q_i = (D_a)/(\pi^\star V^\star D_e) \tag{2}$$

where $D_a = \langle 5d \| r \| 5f \rangle$ is the matrix element for the $5d \rightarrow 5f$ absorption, and $D_e = \langle 5f \| r \| e \rangle$ is the matrix element for $5f$ photoemission (see Fig. 2.) If the transition probabil-

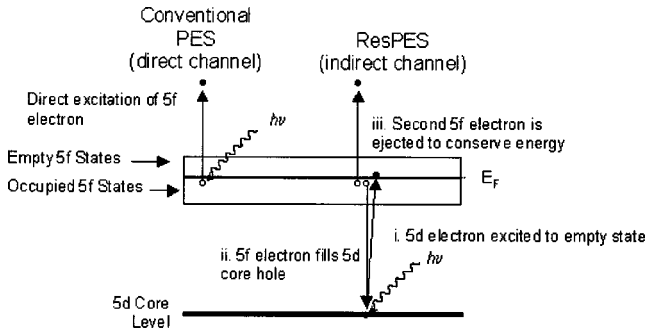

FIG. 2. Schematic of the resonant photoemission process. Photoemission is a ''photon in–electron out'' process. In conventional photoelectron spectroscopy, a single electron/single channel is involved. In RESPES, additional indirect channels with multiple electrons can participate, increasing the cross section and sensitivity of the process.

ity for absorption ($5d \rightarrow 5f$) is much larger than for direct photoemission ($5f \rightarrow e$), the Fano parameter q is large, resulting in line shapes that are rather symmetric. As q approaches infinity, the Fano line shape goes over into a Lorentzian. It is important to note that Γ and q only have a simple meaning for a single line interacting with a continuum. In the presence of a multiplet structure, intermediate states of the same symmetry interfere with each other. In this calculation, the interference was explicitly taken into account by diagonalization of the Hamiltonian for the connected final states, $5d^9 5f^{n+1} \leftrightarrow 5d^{10} 5f^{n-1} + e$. Additional details of the spectral simulations are available elsewhere.[30–34]

III. Pu SAMPLE QUALITY AND PHASE SPECIFICITY

Considering the significant differences between the new alpha and delta samples versus the aged delta sample, it is useful at this point to perform an elemental analysis using a higher photon energy. Shown in Fig. 3 are several wide scans at photon energies of 850 eV. The dominant features are all assigned to Pu $5f$ [(binding energy) (BE) $=0$ eV]; $6p$ (BE $=-16$ and -29 eV), and $5d$ (BE $=-102$ eV), $5p$ (BE $=-210$ eV), and $4f$ (BE $=-421$ and -434 eV). Weaker features can be observed at BE $=-285$ eV [possibly carbon $1s$ (C $1s$) but actually Pu derived] and BE $=-530$ eV (oxygen $1s$ or O $1s$). Unfortunately, in the scans with a photon energy of 850 eV, the O $1s$ peak is obscured by a larger Pu Auger peak at kinetic energy KE $=310$ eV. (There is also another Pu Auger peak at KE $=200$ eV, i.e., with BE near -650 eV at $h\nu = 850$ eV.) Moreover, although the aged delta sample exhibits a significantly different RESPES, the wide scan suggests that all three samples are to a large degree the same in terms of elemental composition, i.e., dominated by Pu features with small O $1s$ peaks. This would seem to rule out one of the proposed explanations for the differences in the aged Pu sample RESPES: surface segregation of the Pu daughter products such as Am. Thus at this point, the remainder of the discussion will focus upon the results for the two new samples, polycrystalline alpha and large crystallite delta. Although very similar in terms of RESPES and wide survey scans, it is possible for the alpha and delta sample to be differentiated.

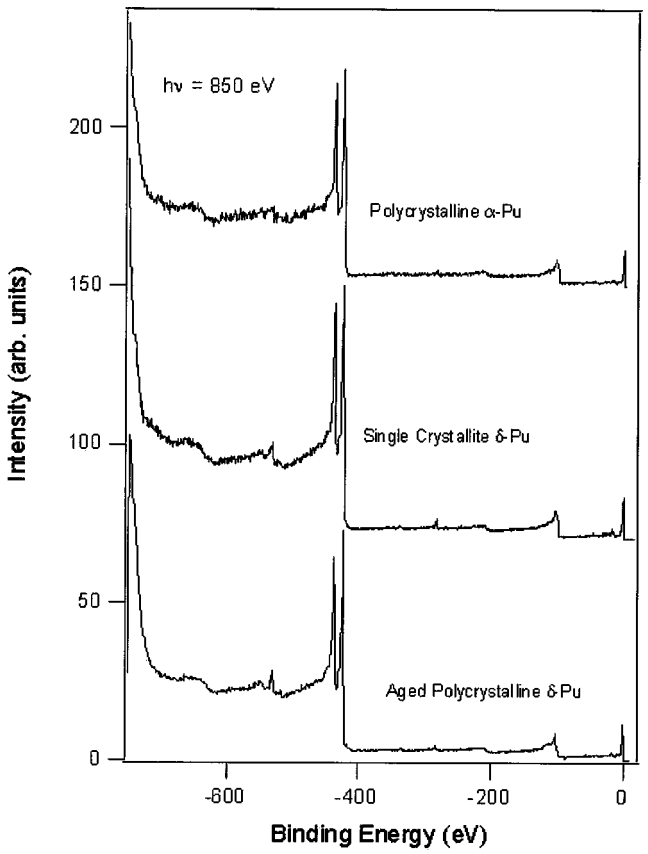

FIG. 3. Pu wide photoemission scans at 850 eV, for a polycrystalline α-Pu (top), single crystallite δ-Pu (middle), and aged polycrystalline δ-Pu (bottom). The bandpass was about 350 meV in these spectra.

The issue of sample quality revolves primarily around the level of surface oxidation. Oxygen has three levels: O $1s$ (BE $=-529$ eV), O $2s$ (BE $=-23$ eV), and O $2p$ (BE $=-5$ eV). Each level has cross sections which can change dramatically with the photon energy, as can the cross sections of the Pu levels. (Below, the cross section calculations of Yeh and Lindau[35] for oxygen and plutonium have been utilized. Unfortunately, the calculations of Yeh and Lindau do *not* include the effects of the $5d$-$5f$ resonance in Pu.) We will present experimental results which demonstrate the tremendous intensity variations in the regime of the resonance, as well as the Cooper minimum. To avoid the problem of quantification in this regime, most of the quantitative analysis will be focussed in other more well-behaved photon energy regimes.

A. Phase differentiation

A number of spectroscopic differences between the alpha and delta phases, particularly with techniques or regimes that favor bulk sensitivity, have been observed. Using total electron yield in x-ray absorption [Fig. 4(a)], a distinct shift between the alpha and delta phases can be discerned. The mean free path for total yield has been estimated to be on the order of 22 Å,[36] thus this is a fairly bulk sensitive measurement.

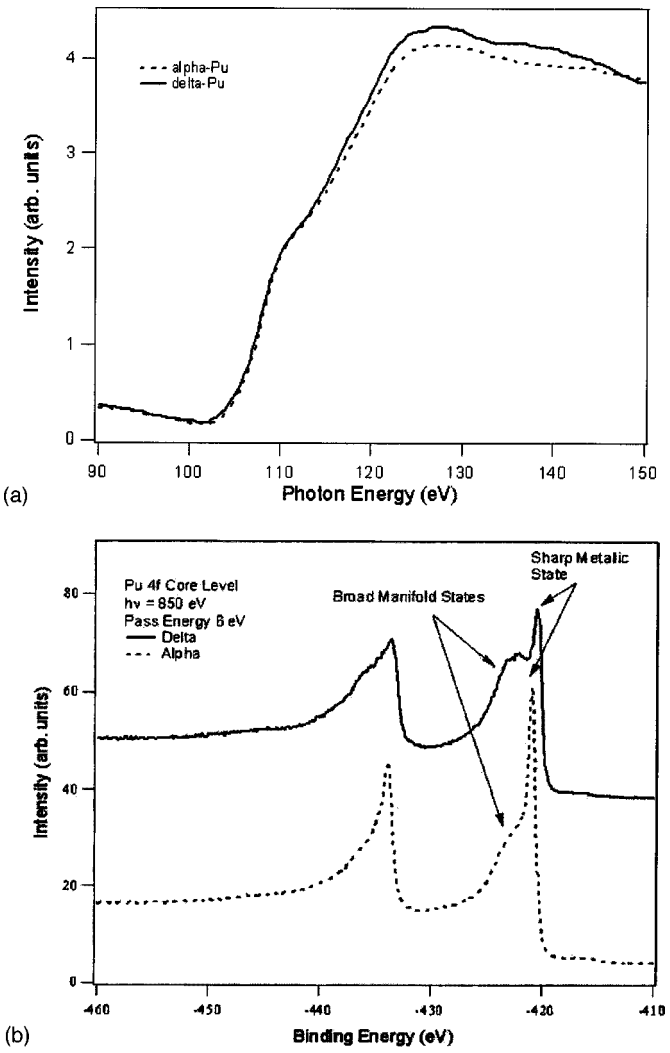

FIG. 4. (a) X-ray absorption of Pu at the $5d$ threshold ($O_{4,5}$), from a large crystallite δ-Pu sample and a polycrystalline α-Pu sample. The instrumental bandpass was 40 meV or better throughout. (b) Core-level photoemission spectra from a large crystallite δ-Pu sample and a polycrystalline α-Pu sample are shown. These spectra were collected with a photon energy of 850 eV and a bandpass of about 350 meV. Note that two large components are visible in each spectral structure; there is a sharp feature at low binding energy, and a broad feature at higher binding energy.

The shift in Pu is very similar to that reported for α-Ce and γ-Ce phases by Wieliczka *et al.*[37] Core level photoemission also provides a mechanism for distinguishing the alpha and delta phases. In Fig. 4(b), there are distinct differences between the alpha and delta $4f$ line shapes, in agreement with a substantial body of previous work by Naegele,[38] Gouder and co-workers,[14–18] and Havela *et al.*[19] Again, because of the fairly high kinetic energy of the electrons (about 400 eV), there is a fair amount of bulk sensitivity here. It has been argued in the past[14–19] that the relative sharpness of the peaks in α-Pu and the large satellite features in δ-Pu are suggestive of delocalization in α-Pu and atomic or electron correlated effects in δ-Pu. Because our samples of Pu are polycrystalline, low energy electron diffraction is not an option.

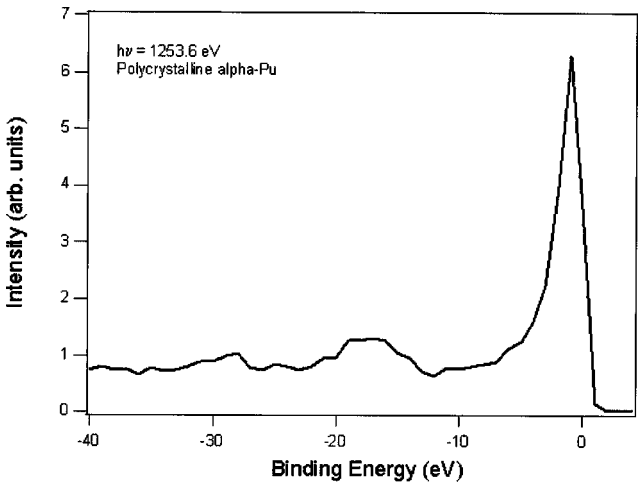

FIG. 5. PES spectrum of α-Pu at $h\nu=1250$ eV. Note the presence of the features associated with the Pu $5f$ (BE 0 eV), Pu $6p3/2$ (BE -16 eV), and Pu $6p1/2$ (BE -29 eV) but the absence of oxygen derived features, e.g., the O $2p$ (BE$=-5$ and -10 eV) and O $2s$ (BE$=-23$ eV). The effective resolution here is degraded below that of the 200–300-meV bandpass quoted for the other Pu spectra, being on the order of 0.6 eV.

B. Sample oxidation estimation via Pu $4f$ level spectra

How do our $4f$ core level spectra compare to those of known oxides? Pu $4f$ spectra of PuO2 and other Pu oxides are available from the literature and useful to compare to our spectra. Courteix *et al.*[26] provide $4f$ core level spectra for a series of oxidation levels and using Mg$K\alpha$ excitation ($h\nu=1254$ eV). [Similar core level spectra can be found in Veal *et al.*,[27] for Al$K\alpha$ excitation ($h\nu=1487$ eV)]. In Courteix *et al.*,[26] spectrum a is for nominally clean delta—Pu, spectra *b*, *c*, and *d* are for increasing oxidation levels, and spectrum *d* corresponds to PuO2. It is immediately obvious that the $4f$ spectra from our delta samples in Fig. 4(b) are qualitatively different than the spectra from the PuO2. (PuO2 has a 4 maximum structure, with separate peaks at BE$=-426$, -433, -439, and -445 eV.) Thus we can establish the bound that our Pu samples are not remotely similar to PuO2. Courteix *et al.* also conveniently supply O $1s$ spectra, calibrated relative to the Pu $4f$ peaks. We shall return to this later, but looking ahead, we will see that the O $1s$ intensities in our spectra at $h\nu=1250$ eV are very much smaller.

C. Oxidation level estimation from valence band spectra ($h\nu=1250$ eV)

How do our valence band spectra at a photon energy corresponding to a Mg$K\alpha$ source (1250 eV) compare to those of known oxides? Again, valence band spectra at $h\nu=1254$ eV for Pu oxides (Courteix *et al.*[26]) and clean Pu (Baptist *et al.*[25]) are available from the literature. Upon examination, it is clear that our spectrum at $h\nu=1250$ eV (shown in Fig. 5) is very similar to that of Baptist *et al.* and very dissimilar to that of the Pu oxides of Courteix *et al.* Note especially the absence of the O $2p$ and O $2s$ peaks from our spectrum at $h\nu=1250$ eV. In the spectra of the Pu oxides of Couteix *et al.* at $h\nu=1254$ eV,[26] there are fairly

strong multiple oxygen-derived peaks BE$=-5$ eV (O $2p$), BE$=-10$ eV (O $2p$), and BE$=-23$ eV (O $2s$). Again, this is an indication that the oxidation of our samples is fairly limited.

D. Quantitative analysis of the O 1s intensity

From the $h\nu=1250$ eV spectrum in Fig. 6, it is immediately obvious that we have only a very small O $1s$ intensity versus that of the Pu oxides of Courteix *et al.*[26] In our $h\nu=1250$ eV spectrum, the O $1s$ peak cannot be seen above the noise. In the PuO2 spectrum of Courteix *et al.*, the O $1s$ peak is approximately one-third the height of the Pu $4f$ peaks. This suggests that we have orders of magnitude less oxygen that the PuO2 sample. To enhance the O $1s$ cross section, we also performed the same measurements at $h\nu=860$ eV. At this photon energy, we can see the O $1s$ (BE $=-530$ eV) and what may be C $1s$ (BE$=-280$ eV). By measuring the relative intensities of the O $1s$ and Pu $4f$ peaks and then correcting for their cross sections (Yeh and Lindau[35]), we can come up with an O/Pu concentration ratio of 0.06 ± 0.06 or $6\%\pm6\%$. The weakness of the O $1s$ feature and uncertainties in the cross section calculations cause the large error bar here.

It should be noted that measurements based upon using the O $1s$ peak are highly preferable to those using the peaks of the O $2p$ and O $2s$ states. This is because (1) the $2p$ and $2s$ states are close enough to the valence regime to be affected by changes in bonding, and (2) the normalization for the measurements in this regime is usually the valence band or $5f$ peaks, the intensity of which may also change with chemical state, emission angle, photon energy, kinetic energy, etc.

Although in the region labeled as C $1s$, the peak at BE $=-280$ eV is actually Pu $5s$ derived, based upon an analysis of the intensity variations of this feature and the Pu $4f$ peaks, using the cross sectional calculations of Yeh and Lindau. Independently, Baptist *et al.* came to a similar conclusion (Pu $5p$ derived).[25]

Finally, why did we use spectra at 860 eV instead of 850 eV? In our first analysis, we used the spectra at $h\nu=850$ eV. (Fig. 3) Unfortunately, at that energy the O $1s$ peak overlaps with a Pu Auger peak, causing the incorrect impression of more oxygen contamination that there actually is. This same Pu Auger peak can also be seen in the $h\nu=1250$ eV spectrum at BE$=-950$ eV. By working at $h\nu=860$ eV, the O $1s$ peak can be isolated from the nearby Auger feature.

E. Photon energy dependence of the O 2p peak

Why does the O $2p$ look so big in the spectra at the Cooper minimum and the $5f$ antiresonance? Obviously, we have some oxygen on the Pu samples. By going to where the Pu $5f$ cross section is very small, it is possible for us to accentuate the oxygen based features such as the O $2p$ peak at BE$=-6$ eV. Two places where the $5f$ cross section is the smallest are the antiresonance at $h\nu=102$ eV and the Cooper minimum at $h\nu=220$ eV (Fig. 7 and Yeh and Lindau[35]).

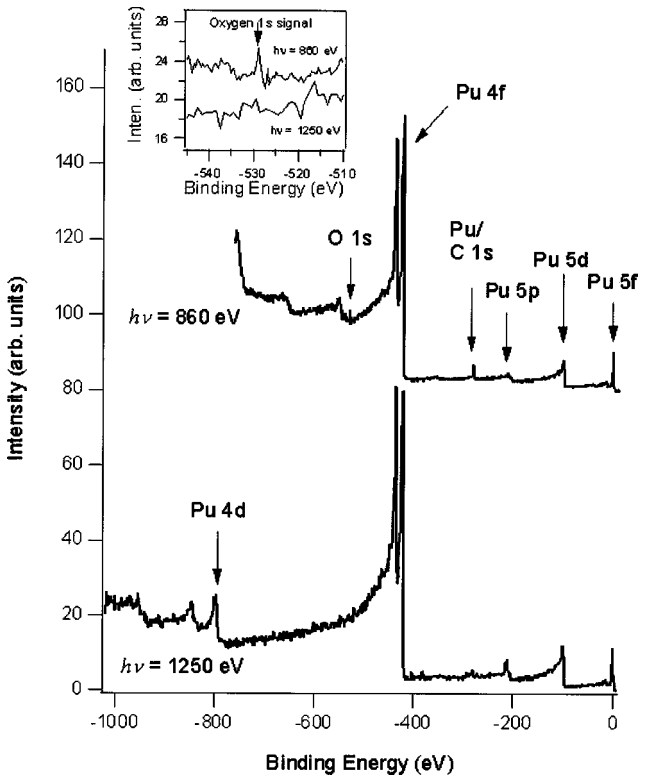

FIG. 6. Wide scans of δ-Pu at photon energies of 860 eV (bandpass of 0.35 eV) and 1250 eV (bandpass of about 0.6 eV) are shown here. The oxygen (O $1s$, binding energy of -530 eV) is much more easily observed at 860 eV (black curves) than at 1250 eV (red curves). The inset shows an enlargement of that region for each photon energy.

Looking at the resonant photoemission spectroscopy of Pu in Fig. 1 and the x-ray absorption in Fig. 4, it is easy to see the low intensity of the Pu $5f$ states at the anti-resonance at $h\nu=102$ eV. At the Cooper minimum, the Pu $5f$ cross section is about 1/500 of its maximum value. In fact, note the

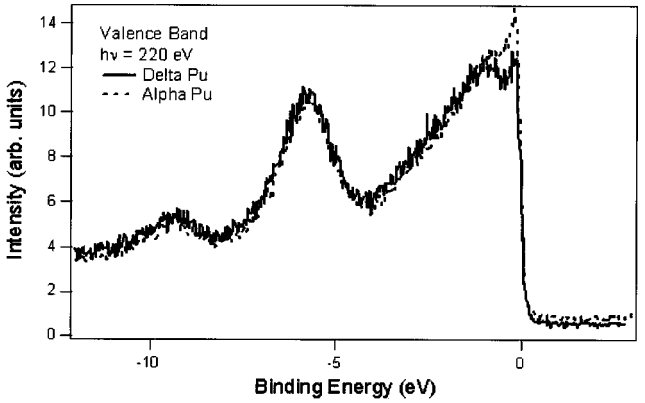

FIG. 7. Photoemission EDCs near the Cooper minimum of the Pu $5f$ states are shown here, for both the large crystallite δ-Pu sample ($h\nu=220$ eV) and the polycrystalline α-Pu sample ($h\nu=225$ eV). Here at the Cooper minimum, the Pu $5f$ intensity is diminished and the oxygen peaks at -5 and -10 eV are relatively enhanced. The instrumental bandpass was 0.1 eV or lower for both of these spectra.

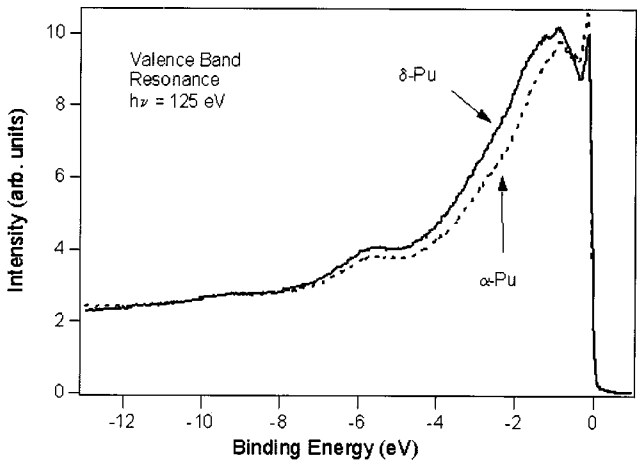

FIG. 8. EDCs of the large crystallite δ-Pu sample and a polycrystalline α-Pu sample at a photon energy of 125 eV are shown. Note the sharp rise at the Fermi edge, indicative of the 100-meV bandpass. The bandpass contribution (100 meV or less) and the thermal contribution (about 0.113 eV at room temperature) combine to give a width at the Fermi Edge (BE$=0$ eV) of about 0.2 eV.

second O $2p$ feature in Fig. 7 at BE$=-10$ eV, similar to that observed in the spectrum of PuO2 at $h\nu=1254$ eV by Courteix *et al.*[26]

The valence band spectra at the Cooper minimum and the antiresonance can cause the impression that samples were dirtier than they really were, but this is incorrect. The better analysis is based upon the Pu $4f$ and O $1s$ peaks, as described above.

F. Why are the valence band spectra for the alpha and delta samples so similar? Shouldn't they be more different?

Havela, Gouder, Wastin, and Rebizant[19] have shown that a deltalike reconstruction forms on alpha Pu if the temperature is room temperature or above. Our gentle annealings (T about 373 K) were sufficient to cause the reconstruction on our alpha samples. For this reason, our Pu valence band spectra are qualitatively similar for the two phases, α-Pu and δ-Pu. (E.g., see Fig. 8.) It is worthwhile to note how small O $2p$ peak at BE$=-6$ eV is at this photon energy. Additionally, it should be mentioned that while the interpretations are significantly different, our observation of spectral similarities for α-Pu and δ-Pu is consistent with the observations of Arko *et al.*[9]

G. Summary result of the sample quality analysis

Although our samples are not quite as clean as those of both Gouder and co-workers[14–19] and Joyce *et al.*,[39] we are in the right regime. Because these are the only known synchrotron-radiation-based PES and x-ray absorption results for Pu and because the sample quality is fairly good, it is worth continuing the analysis.

IV. DISCUSSION AND RESULTS

A. Pu experiments

The spectroscopic experiments described here are based upon x-ray absorption and PES. A diagrammatic summary of PES and resonant PES (RESPES) can be found in Fig. 2, for the energy levels corresponding to Pu. In a RESPES experiment, the valence band spectrum is collected as the photon energy is ramped through a core level absorption edge. In the case of Pu, the photon energy was scanned through the $O_{4,5}$ $(5d)$ absorption edge. Thus, the result is the $5d5f5f$ resonant photoemission decay from Pu metal. The final state can be reached by an x-ray absorption-Coulomb decay process, $5d^{10}5f^n+h\nu\rightarrow 5d^9 5f^{n+1}\leftrightarrow 5d^{10}5f^{n-1}+e$, and by direct photoemission, $5d^{10}5f^n+h\nu\rightarrow 5d^{10}5f^{n-1}+e$, where e is a photoelectron in a continuum state which has no interaction with the ionic state left behind. Interference between the different pathways results in asymmetric absorption features in the measured spectra. Our Pu studies have been performed with synchrotron radiation as the excitation, and are meant to complement earlier Pu studies performed with laboratory sources as the excitation.[9,14–28]

Photoelectron spectroscopy is a ''photon in, electron out'' process. Often, it can be simplified down to a single electron phenomenon, where the energy of the photon is absorbed and transferred over entirely to a single electron, while all other ''spectator'' electrons essentially remain frozen. An advantage of this is its simplicity of interpretation. But in many systems, it is possible to induce a process with heightened sensitivity and significantly increased cross sections: resonant photoemission (ResPes).[30,32–34,40] Here, a second set of indirect channels open up, which contribute in concert with the original or direct channel of simple photoemission. Shown in Fig. 1 are resonant photoemission results from polycrystalline α-Pu, single crystallite (large grain polycrystalline) δ-Pu, and aged polycrystalline δ-Pu. One salient result is that it is abundantly clear that all of the Pu states at and near the Fermi level have a strong $5f$ character. The overall spectral envelopes are approximately the same, as expected for three samples which are primarily Pu. Nevertheless, significant differences can be observed between the new, purified α and δ samples versus the aged δ-Pu, particularly at the Fermi energy and near a photon energy of 130 eV. These results suggest that the valence electronic structure of Pu is dependent upon its phase and chemical state. Nevertheless, overall the three sets of spectra strongly resemble each other and confirm the observation of Pu $5f$ RESPES.

Resonant photoemission has a distinct line shape as a function of photon energy. This can be seen the photoemission results of Fig. 1, particularly in the data for the zone refined alpha and delta samples. After an initial preresonance regime (near $h\nu=90$ eV), there is an antiresonance (near $h\nu=100$ eV) followed by a resonance (maximum near $h\nu=125$ eV), with an intensity which quickly diminishes as the photon energy increases from 130 to 150 eV. (These results at higher energies are in disagreement with the calculations of Molodtsov *et al.*,[41] although the emphasis in their work is upon the behavior near threshold.) Some of this behavior is mimicked in the x-ray absorption measured near the $5d$ threshold (BE$=-102$ eV), shown in the top panel of Fig. 4. Note also, how different the absorption results are for the Pu $5d$ threshold (near 102 eV) versus the Pu $4d5/2$ threshold (Fig. 9, near 800 eV). While the RESPES and $5d$ absorption results for the alpha and delta samples

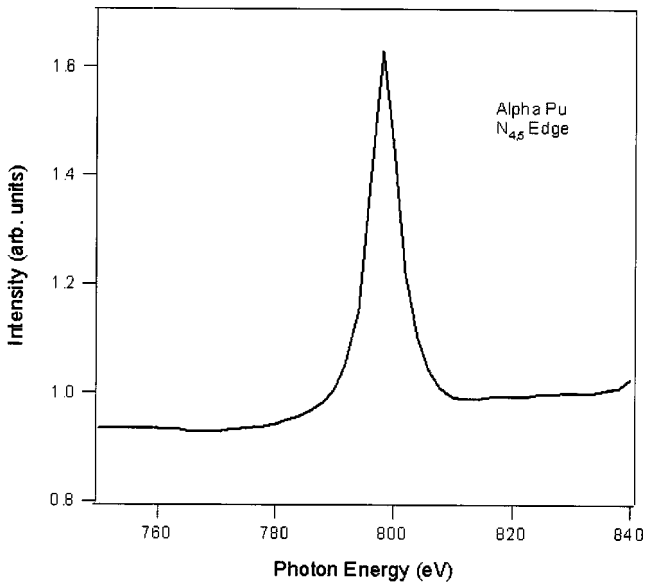

FIG. 9. X-ray absorption spectrum of α-Pu at the $4d$ ($N_{4,5}$) threshold. Only the Pu $4d$ 5/2 peak is shown. The bandpass was 0.4 eV or better throughout.

(Figs. 1 and 4) exhibit some differences, to a large extent they are quite similar. This can also be seen in the detailed comparison of the electron distribution curves (EDCs), which are plots of photoemission intensity versus electron binding energy for a fixed photon energy. An example of this is shown in Fig. 8. A sharp peak near the Fermi energy is followed by a minimum, then a wide peak with a maximum near a binding energy of BE$=-1$ eV. The similarity of the RESPES, EDCs and $5d$ absorption for alpha and delta Pu is consistent with the recent hypothesis of surface reconstruction of alpha into a deltalike surface.[14,19] Small additional peaks at BE$=-6$ and -10 eV can be seen, which are attributable to the O $2p$ features of Pu oxide, especially PuO2. (These assignments were also discussed in Sec. III above.) The high resolution (approximately 100-meV bandpass or better) of the Pu RESPES experiment is confirmed by the sharp Fermi edge jump observed in these spectra.

Another aspect of RESPES in f-electron systems is the possibility of a parallel effect in the nearby p state emission. In the case of the Pu $5f$ RESPES, the related effect would be in the Pu $6p$ states. Figure 10 shows a series of EDCs at photon energies of 100 eV (antiresonance), 125 eV (resonance), 180 eV (off resonance), and 225 eV (the $5f$ Cooper minimum[35]). In the spectra are six major peaks, whose intensities vary distinctly with photon energy. The six are near binding energies of 0 eV (Pu $5f$), -5 eV (oxide O $2p$), -10 eV (PuO2 O $2p$), -16 eV (Pu $6p3/2$), -23 eV (O $2s$), and -29 eV (Pu $6p1/2$). At resonance (near $h\nu=125$ eV), the Pu $5f$, Pu $6p3/2$, and Pu $6p1/2$ peaks are strong, overshadowing the smaller O $2s$ and O $2p$ peaks. Off-resonance, at $h\nu=180$ eV, the Pu $5f$, Pu $6p3/2$, and Pu $6p1/2$ peaks appear to have similar intensity ratios, but the O $2p$ peaks have increased slightly relative to the Pu features. However, at antiresonance ($h\nu=100$ eV) and at the Cooper minimum ($h\nu=225$ eV), O $2p$ peak intensities are substantially increased relative to the Pu $5f$ peak height, near the Fermi energy (BE$=0$ eV). Interestingly, the $6p$:$5f$ ratio appears to be larger at $h\nu=225$ eV than at $h\nu=100$ eV. This is to be expected, since both the $6p$ and $5f$ intensities should be suppressed at the antiresonance ($h\nu=100$ eV) but only the $5f$ (and not the $6p$) intensity should be reduced at the $5f$ Cooper minimum at $h\nu=225$ eV. (The relationship between the O $2p$ and O $2s$ intensities is complicated by the fact that while the O $2p$ cross section is significantly higher at $h\nu<100$ eV and both the O $2p$ and O $2s$ cross sections decrease monotonically over the photon energy range of 100–300 eV, it appears that the O $2s$ and O $2p$ cross section values cross in the vicinity of $h\nu=200$ eV.[35] (It should be noted that the calculations of Yeh and Lindau[35] do not include RESPES effects over the photon energy range of 90–160 eV.)

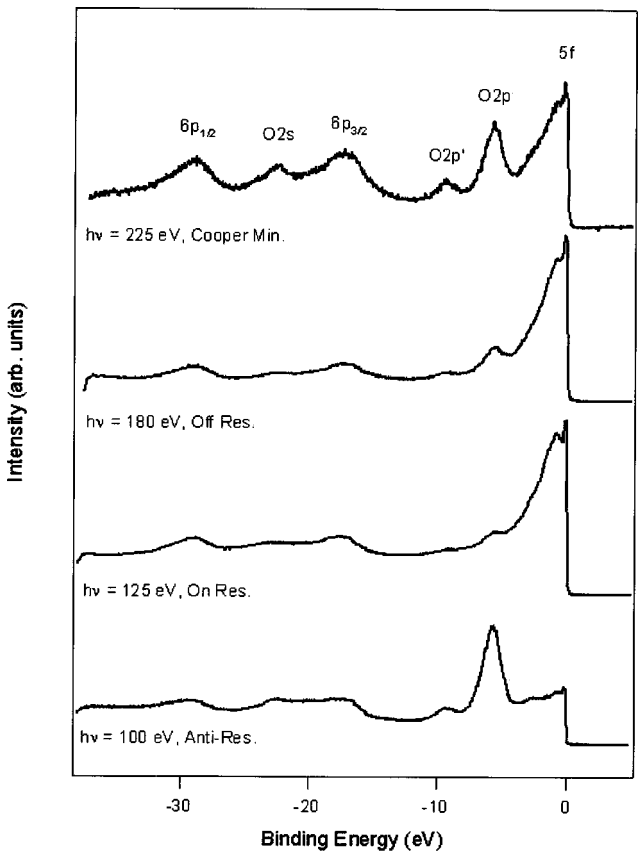

FIG. 10. EDCs of alpha Pu at photon energies of 100 eV (antiresonance, bottommost), 125 eV (on resonance, second from bottom), 180 eV (off resonance, second from top), and 225 eV (Cooper minimum, topmost). The experimental bandpass was 100 meV or better throughout.

As mentioned above, the spectra for the new alpha and delta samples are quite similar. This extends to the EDCs at the Cooper minimum photon energy of 220 eV. As shown in Fig. 7, even the oxygen-Pu ratios are similar.

B. Gd experiment and theory

At this point it is useful to compare the RESPES of the Pu $5f$ and Pu $6p$ states with that in the Gd $4f$ and $5p$ states,

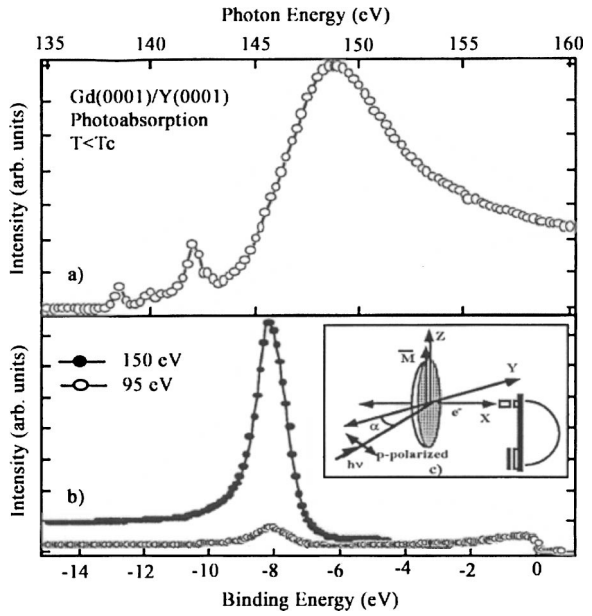

FIG. 11. The x-ray absorption and photoemission of Gd thin films. In the upper panel we show x-ray absorption near the $4d$ threshold, showing the prepeak structure at 137 and 142 eV and the giant resonance at 148 eV. Below is $4f$ photoemission, both on (150 eV) and off (95 eV) resonance. The inset shows the experimental geometry.

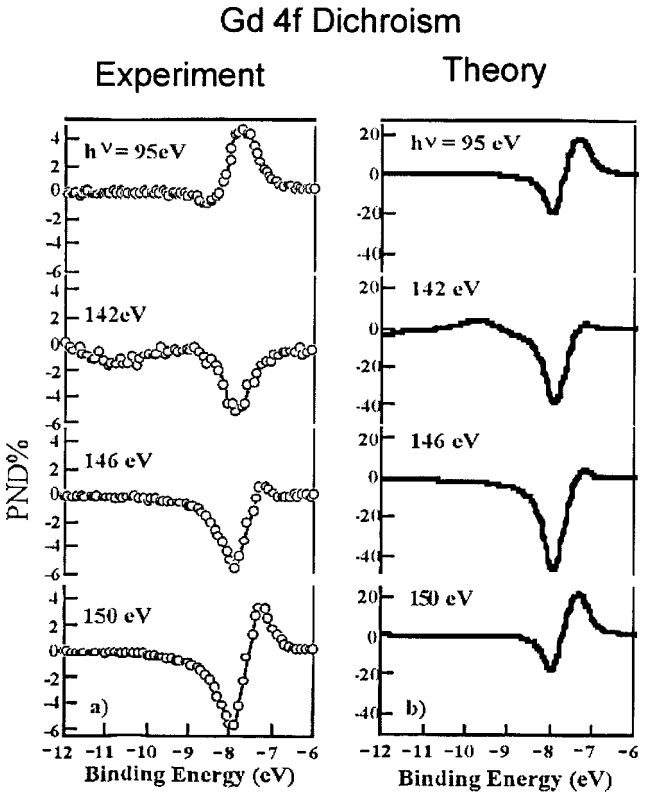

FIG. 12. A series of experimental and theoretical Gd $4f$ photoemission dichroism spectral difference curves. On the left are the experimental curves, on the right are the theory curves. From the top, the photon energies are 95, 142, 146, and 150 eV. PND stands for peak normalized difference, where the dichroism difference at each binding energy is divided by the sum of the two intensity maxima, one from each spectral pair. (Not shown; following Ref. 4.) The photon energy of 150 eV is ''on'' resonance and that of 95 eV is ''off'' resonance.

respectively.[30] Shown in Fig. 11 are photoemission spectra of the Gd $4f$ states on resonance ($h\nu=150$ eV) and off resonance ($h\nu=95$ eV) as well as an x-ray absorption curve for Gd near near the Gd $4d$ thresholds (near BE$=-145$ eV). One aspect which is immediately obvious when comparing the Gd x-ray absorption near the $4d$ threshold with the Pu x-ray absorption near the Pu $5d$ threshold is that the Gd has a fine structure or prepeaks below threshold but Pu does not. This is the first of many indicators that the Pu $5f$ states are different from the Gd $4f$ states. In the case of the Gd $4f$ and $5p$ RESPES one way to get more detailed information is to perform an x-ray magnetic linear dichroism experiment, where the sample is remnantly magnetized first in one direction and then in the reversed direction.[30] (See the inset in Fig. 11.) Spectra can be collected for each of these configurations: the spectral differences are then a measure of the magnetic dichroism. Shown in Fig. 12 are the Gd $4f$ dichroic differences for a series of photon energies. Furthermore, using an atomic model with angular momentum coupling[30,32–34] it is possible to simulate these differences and their photon energy dependences almost exactly. (See Fig. 12.) Similarly, the model works very well for the Gd $5p$ states, as can be seen in Fig. 13. Here, the photon energy dependence, fine structure, and magnetic dependences exhibited by the experimental results are matched by the theoretical simulations. Again, another manifestation of the more delocalized nature of the Pu states can be seen here. While the Gd $5p$ states show a plethora of fine structure, the Pu $6p$ states are smooth and structureless in Fig. 10. The Pu results suggest a more metallic or delocalized shielding of the p hole final state, with a loss of the fine structure which is present in rare earth elements such as Gd. This fine structure in the rare earths is sometimes attributed to angular momentum coupling.[32] It also suggests strongly that Pu is nonmagnetic, with a small or zero moment per atom.

C. Comparison of Pu experiment to theory

Now we will compare the experimental results to calculations based upon an atomic model. Theoretically, α-Pu should be more free-electron-like than δ-Pu. Here, we will be looking for trends instead of quantitative agreement. In any case, it is highly useful for us to begin the analysis by comparing our Pu experimental results to an atomic picture of $5f$ RESPES.

Constant initial state (CIS) spectra, with a fixed binding energy and a variable photon energy, are a measure of the absorption and resonant photoemission. (These are slices through the plots in Fig. 1, with fixed binding energies.) Both Pu experimental and calculated atomic results are shown in Fig. 14. The calculated $5d$ absorption spectrum (BE $=-12.0$ eV) displays a broad structure with roughly three features. The separation into these distinct features is mainly due to the *df* and *ff* Coulomb interactions. The two features at lower energy have mainly $J=7/2$ and 5/2 characters, while

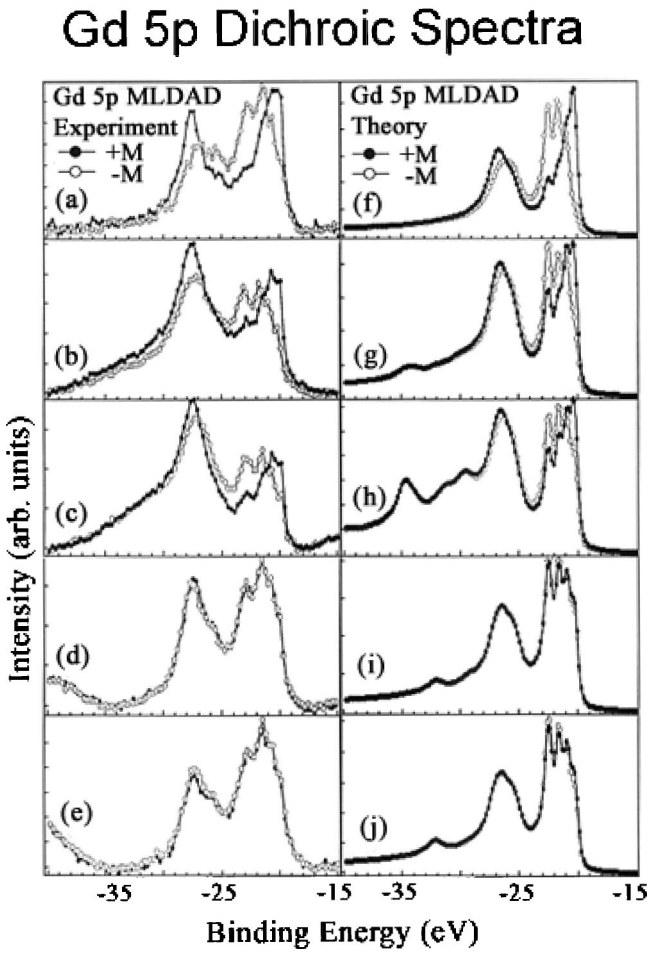

FIG. 13. A series of experimental and theoretical Gd $5p$ photoemission spectra (for the two opposite magnetization directions). (a) $h\nu=137$ eV, experimental. (b) $h\nu=140$ eV, experimental. (c) $h\nu=142$ eV, experimental. (d) $h\nu=149.6$ eV, experimental. (e) $h\nu=151$ eV, experimental. (f) $h\nu=137$ eV, theory. (g) $h\nu=140$ eV, theory. (h) $h\nu=142$ eV, theory. (i) $h\nu=149.6$ eV, theory. (j) $h\nu=151$ eV, theory. EDC is the energy distribution curve. The experimental spectra are EDCs where the photon energy is held constant and the kinetic energy is scanned. The relative intensities of the experimental curves were determined by normalizing to the valence band intensities and then correcting for the valence band cross sections. (See Ref. 30.)

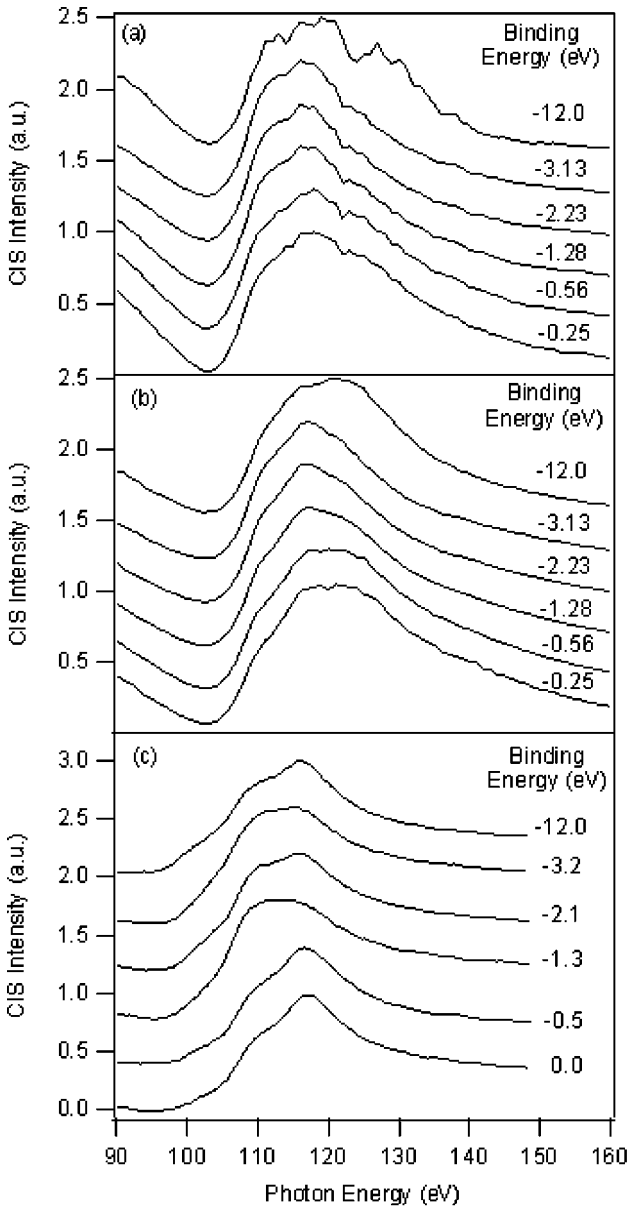

FIG. 14. The constant initial state spectra (CIS) are shown: (a) α-Pu, (b) δ-Pu, and (c) atomic theory. (a) The calculated spectra are shown at binding energies of 0.0, -0.5, -1.3, -2.1, -3.2, and -12.0 eV. The experimental spectra are shown at similar binding energies. Note that in both the calculated and measured δ-Pu spectra, the intensity of the second and third peaks switch as the binding energy is increased.

the feature at higher energy has mainly $J=3/2$ character. The line broadening is due to the decay where the Hartree-Fock value of the half-width Γ is about 3.5 eV. Other decay channels, such $5d5f6s$, $5d5f6p$, $5d6p6p$, and $5d6s6p$, were taken into account in the calculation by including an additional Lorentzian of width $\Gamma_0=1$ eV. In the calculated spectra, the strong interference between the direct photoemission and the decay makes the absorption structures asymmetric with an intensity minimum around 97 eV due to the Fano anti-resonance. The experimental CIS spectra from δ-Pu show a similar splitting into two peaks with a separation of about 8 eV (117 and 125 eV) and a possible shoulder at lower energy. In a configuration interaction model, these satellites can be ascribed to configurations $5d^9\,5f^n$. With different n in x-ray absorption (but not in photoemission), the satellite intensities are usually small and a single-configuration approximation is often valid.[32–34] The reason for this is that after $5d\rightarrow5f$ excitation, the $5d$ core hole is efficiently screened by the additional $5f$ electron. The most successful application of the atomic model is its ability to reproduce the relative intensities of the second (theory 110

eV, experiment 117 eV) and third peaks (118 and 125 eV) in the data. The third peak is originally more intense than the second peak. As the binding energy increases (-1.3 eV), the second peak becomes more intense than the third. As the binding energy is further increased the intensities reverses again. This suggests the presence of a remnant of atomic structure in the δ-Pu. This similarity between theory and experiment was not as well observed in the CIS spectra from α-Pu, but still appears to be present. The diminishment of the effect in α-Pu is possibly due to the assumed greater delocalization of the *f* electrons in the α-Pu sample. Finally, comparisons between experiment and theory along the other axis, using plots of intensity versus binding energy for various photon energies, were even less successful.

V. SUMMARY

High quality RESPES spectra of α-Pu and δ-Pu have been collected and compared to the results of a similar experimental investigation of Gd Significant agreement has been found to the results of atomic spectral simulations. Nevertheless, it is clear that an atomic model alone will not suffice to explain the observations of $5f$ resonant photoemission in Pu. One salient result is that it is abundantly clear that all of the Pu states at and near the Fermi level have a strong $5f$ character. Supporting core level measurements and x-ray absorption have been made which confirm the α-Pu and δ-Pu are different. Comparison of Gd $5p$ and Pu $6p$ results suggest a more metallic, less atomic behavior in Pu relative to Gd, and also that the Pu has much smaller, if any, magnetic moment per atom. In the future, refined sample preparation and enhanced inclusion of delocalization effects in the theory will be required for further phase specific analyses. Furthermore, more extensive analysis will be necessary to differentiate between the various models for $5f$ photoemission, such as those based upon multiplet formation[42] and potential internal magnetic spitting[43,44] and spin orbit effects.[45]

ACKNOWLEDGMENTS

This work was performed under the auspices of the U.S. Department of Energy by LLNL (Contract No. W-7405-Eng-48), LANL (Contract No. W-7405-ENG-36) and LBNL (Contract No. DE-AC03-76SF00098). The Spectromicroscopy Facility (Beamline 7.0) and the Advanced Light Source were built and are supported by the DOE Office of Basic Energy Research. The authors wish to thank Jason Lashley and Michael Blau for synthesis of the Pu samples. T. Zocco contributed immensely to the Pu experiments at the ALS. D.A. Arena aided in some of the Pu data analysis. F.O. Schumann, S. Mishra, and T. Cummins contributed to the Gd data collection and analysis.

*Electronic address: Tobin1@LLNL.Gov; Tel: 925-422-7247; FAX: 925-423-7040.

[1] S. S. Hecker, MRS Bull. **26**, 667 (2001).
[2] B. D. Wirth, A. J. Schwartz, M. J. Fluss, M. J. Caturla, M. A. Wall, and W. G. Wolfer, MRS Bull. **26**, 679 (2001).
[3] B. Johansson, Phys. Rev. B **11**, 2740 (1975).
[4] B. R. Cooper *et al.*, in *Handbook on the Physics and Chemistry of Actinides*, edited by A. J. Freeman and G. H. Lander (Elsevier, Amsterdam, 1985), Vol. 2.
[5] P. Soderlind, Adv. Phys. **47**, 956 (1998), and references therein.
[6] P. Soderlind *et al.*, Phys. Rev. B **55**, 1997 (1997).
[7] D. C. Wallace *et al.*, Phys. Rev. B **58**, 15 433 (1998).
[8] W. A. Harrison, Phys. Rev. B **64**, 235112 (2001).
[9] A. J. Arko, J. J. Joyce, L. Morales, J. Wills, J. Lashley, F. Wastin, and J. Rebizant, Phys. Rev. B **62**, 1773 (2000).
[10] S. Y. Savrasov, G. Kotliar, and E. Abrahams, Nature (London) **410**, 793 (2001).
[11] R. C. Albers, Nature (London) **410**, 759 (2001).
[12] S. Y. Savrasov and G. Kotliar, Phys. Rev. Lett. **84**, 3670 (2000).
[13] P. Soderlind, Europhys. Lett. **55**, 525 (2001).
[14] T. Gouder *et al.*, Phys. Rev. Lett. **84**, 3378 (2000).
[15] T. Gouder *et al.*, MRS Bull. **26**, 684 (2001).
[16] T. Gouder *et al.*, Europhys. Lett. **55**, 705 (2001).
[17] T. Gouder, J. Electron. Spectrosc. Relat. Phenom. **101–105**, 419 (2000).
[18] T. Gouder, J. Alloys Compd. **271–273**, 841 (1998).
[19] L. Havela, T. Gouder, F. Wastin, and J. Rebizant, Phys. Rev. B **65**, 235118 (2002).
[20] A. J. Arko *et al.*, J. Alloys Compd. **271–273**, 826 (1998).
[21] A. J. Arko *et al.*, J. Alloys Compd. **286**, 14 (1999).
[22] J. Joyce *et al.*, Surf. Interface Anal. **26**, 121 (1998).
[23] L. E. Cox *et al.*, Phys. Rev. B **46**, 13 571 (1992).
[24] L. E. Cox, Phys. Rev. B **37**, 8480 (1988).
[25] R. Baptist *et al.*, J. Phys. F: Met. Phys. **12**, 2103 (1982).
[26] D. Courteix *et al.*, Solid State Commun. **39**, 209 (1981).
[27] B. W. Veal *et al.*, Phys. Rev. B **15**, 2929 (1977).
[28] D. T. Larson, J. Vac. Sci. Technol. **17**, 55 (1980).
[29] J. D. Denlinger *et al.*, Rev. Sci. Instrum. **66**, 1342 (1995).
[30] S. R. Mishra *et al.*, Phys. Rev. Lett. **81**, 1306 (1998); J. Vac. Sci. Technol. A **16**, 1348 (1998); **17**, 1313 (1999).
[31] J. Terry, R. K. Schulze, J. D. Farr, T. Zocco, K. Heinzelman, E. Rotenberg, D. K. Shuh, G. van der Laan, D. A. Arena, and J. G. Tobin, Surf. Sci. Lett. **499**, L141 (2002); J. Tobin, D. A. Arena, B. Chung, P. Roussel, J. Terry, R. K. Schulze, J. D. Farr, T. Zocco, K. Heinzelman, E. Rotenberg, and D. K. Shuh, J. Nucl. Sci. Technol. **S3**, 98 (2002).
[32] G. van der Laan *et al.*, Phys. Rev. B **59**, 8835 (1999).
[33] G. van der Laan *et al.*, Phys. Rev. B **46**, 9336 (1992).
[34] G. van der Laan *et al.*, Phys. Rev. B **33**, 4253 (1986).
[35] J. J. Yeh and I. Lindau, At. Data Nucl. Data Tables **32**, 1 (1985).
[36] P. Bedrossian *et al.*, in *Applications of Synchrotron Radiation Techniques to Materials Science III*, edited by L. J. Terminello, S. M. Mini, H. Ade, and D. L. Perry, MRS Symposia Proceedings No. 437 (Materials Research Society Pittsburgh, 1996), p. 79.
[37] D. Wieliczka, J. H. Weaver, D. W. Lynch, and C. G. Olson, Phys. Rev. B **26**, 7056 (1982).
[38] J. R. Naegele, J. Nucl. Mater. **166**, 59 (1989); *Electronic Structure of Solids: Photoemission Spectra and Related Data*, edited byA. Goldmann and E. Koch, Landolt-Bornstein, New Series, Group III, Vol. 23 (Springer-Verlag, Berlin, 1994).

[39] J. Joyce, (private communication), Bull. Alloy Phase Diagrams **47**, 960 (2002).
[40] K. Starke *et al.*, Phys. Rev. B **55**, 2672 (1997).
[41] Molodtsov *et al.*, Phys. Rev. Lett. **87**, 017601 (2001).
[42] F. Gerkin and J. Schmidt-may, J. Phys. F: Met. Phys. **13**, 1571 (1983).
[43] A. Mavromaras, Ph.D thesis, Darmstadt Technical University, 1998.
[44] M. S. S. Brooks (private communication).
[45] K. T. Moore *et al.*, Phys. Rev. Lett. **90**, 196404 (2003).